Article

Multifocal Fluorescence Microscope for Fast Optical Recordings of Neuronal Action Potentials

Matthew Shtrahman,[1,2] Daniel B. Aharoni,[2] Nicholas F. Hardy,[1] Dean V. Buonomano,[1,3] Katsushi Arisaka,[4] and Thomas S. Otis[1,*]

[1]Department of Neurobiology and [2]Department of Neurology, David Geffen School of Medicine, University of California Los Angeles, Los Angeles, California; and [3]Department of Psychology and [4]Department of Physics, University of California Los Angeles, Los Angeles, California

ABSTRACT   In recent years, optical sensors for tracking neural activity have been developed and offer great utility. However, developing microscopy techniques that have several kHz bandwidth necessary to reliably capture optically reported action potentials (APs) at multiple locations in parallel remains a significant challenge. To our knowledge, we describe a novel microscope optimized to measure spatially distributed optical signals with submillisecond and near diffraction-limit resolution. Our design uses a spatial light modulator to generate patterned illumination to simultaneously excite multiple user-defined targets. A galvanometer driven mirror in the emission path streaks the fluorescence emanating from each excitation point during the camera exposure, using unused camera pixels to capture time varying fluorescence at rates that are ~1000 times faster than the camera's native frame rate. We demonstrate that this approach is capable of recording Ca^{2+} transients resulting from APs in neurons labeled with the Ca^{2+} sensor Oregon Green Bapta-1 (OGB-1), and can localize the timing of these events with millisecond resolution. Furthermore, optically reported APs can be detected with the voltage sensitive dye DiO-DPA in multiple locations within a neuron with a signal/noise ratio up to ~40, resolving delays in arrival time along dendrites. Thus, the microscope provides a powerful tool for photometric measurements of dynamics requiring submillisecond sampling at multiple locations.

INTRODUCTION

One of the great challenges in neuroscience is to understand how patterns of electrical activity in networks of neurons are linked to brain function. Optical techniques overcome several of the shortcomings of electrophysiological approaches and offer many unique features for measuring activity in neuronal networks, because light can be delivered and sensed noninvasively on temporal and spatial scales that span several orders of magnitude. In addition, optical probes that track neural activity (1,2), including organic fast voltage sensors (3,4) and genetically encoded voltage sensors (5–7), have been developed offering great promise for studying neuronal dynamics. However, developing microscopy techniques that have several kHz bandwidth necessary to reliably capture action potentials (APs) in networks of cells in parallel remains a significant challenge (4,8,9).

Measurements of phenomena with fast dynamics reported via fluorescent probes are nearly always photon limited (9,10), and scanning techniques such as confocal microscopy and two-photon microscopy typically collect light from only a single point in the tissue at a time. Although they offer superior background rejection due to three-

dimensional localization of excitation, even multiplexing (11) and rapid scanning techniques (12) must compromise frame rate or sampling area for dwell time and signal/noise ratio (SNR). Unfortunately, attempts to overcome this photon dilemma by increasing the intensity of the excitation light source are offset by fluorescent probe saturation, photodamage, and photobleaching, which increase with excitation power faster than the number of emitted photons and the corresponding decrease in relative shot noise (13–15).

Multifocal illumination strategies have been proposed in both single and multiphoton microscopy to reduce or eliminate scanning, resulting in increased pixel dwell times and SNR, without compromising frame rate (13). In particular, phase modulating spatial light modulators (SLMs) are capable of efficiently producing multiple excitation spots at arbitrary locations within a sample by shaping the wavefront of coherent laser light (16,17). The fluorescent signals emanating from these excitation spots are imaged in parallel onto a camera. Although both commercial charge-coupled device and complementary metal-oxide-semiconductor (CMOS) camera technologies have experienced significant advances over the past decades, cameras that have fast (>1 kHz) frame rates still suffer tradeoffs resulting in relatively poor light sensitivity, low spatial resolution, or severely restricted regions of interest. There have been recent attempts to overcome some of these limitations (8), but these approaches have not demonstrated sufficient

SNR to capture multifocal, optically reported APs in highly scattering environments such as the brain slice preparation.

Inspired by star trails observed in long exposure images of the night sky, we have developed the fluorescence trails microscope (FTM), which uses a liquid crystal on silicon SLM to generate a custom multifocal pattern or constellation of near diffraction-limited laser spots that excite fluorescently labeled neurons or other targets of interest. Mimicking the star trails created by the Earth's rotation, a large galvanometer-driven mirror streaks the fluorescence emitted from the constellation in one direction across the sensor of a conventional scientific camera (Fig. 1). Thus, the fluorescence fluctuations in time of each dye-labeled neuron are recorded spatially on the sensor as intensity changes along a linear streak. This results in a sampling rate that is approximately the camera frame rate multiplied by the number of pixels within the streak. For example, the FTM accelerates a megapixel (1000 × 1000) camera by ~3 orders of magnitude over its native frame rate.

We apply this tool to record single APs in neurons labeled with either the voltage sensitive dye DiO-DPA (3,18) or the Ca^{2+} sensor Oregon Green Bapta-1 (OGB-1). We demonstrate using DiO-DPA that this approach facilitates detection of single axon potentials in multiple locations within a neuron with SNR up to ~40, resolving delays in arrival time on the order of hundreds of microseconds. We also show that despite the moderately slow response times of Ca^{2+} sensors, this approach can localize the timing of APs in a collection of neurons with ~1 ms resolution. Thus, to our knowledge, this novel microscope design combines tailored spatial illumination and maximal dwell time to optimize temporal resolution and SNR in multisite optical recordings.

MATERIALS AND METHODS

Brain slice preparation

Acute slices were prepared using previously described methods (19). All animal procedures followed the National Institutes of Health guidelines and were approved by the UCLA Institutional Animal Care and Use Committee. Briefly, postnatal day 17 to 45 aged mice (C57 black 6) were used for acute brain slice experiments. Mice were anesthetized with
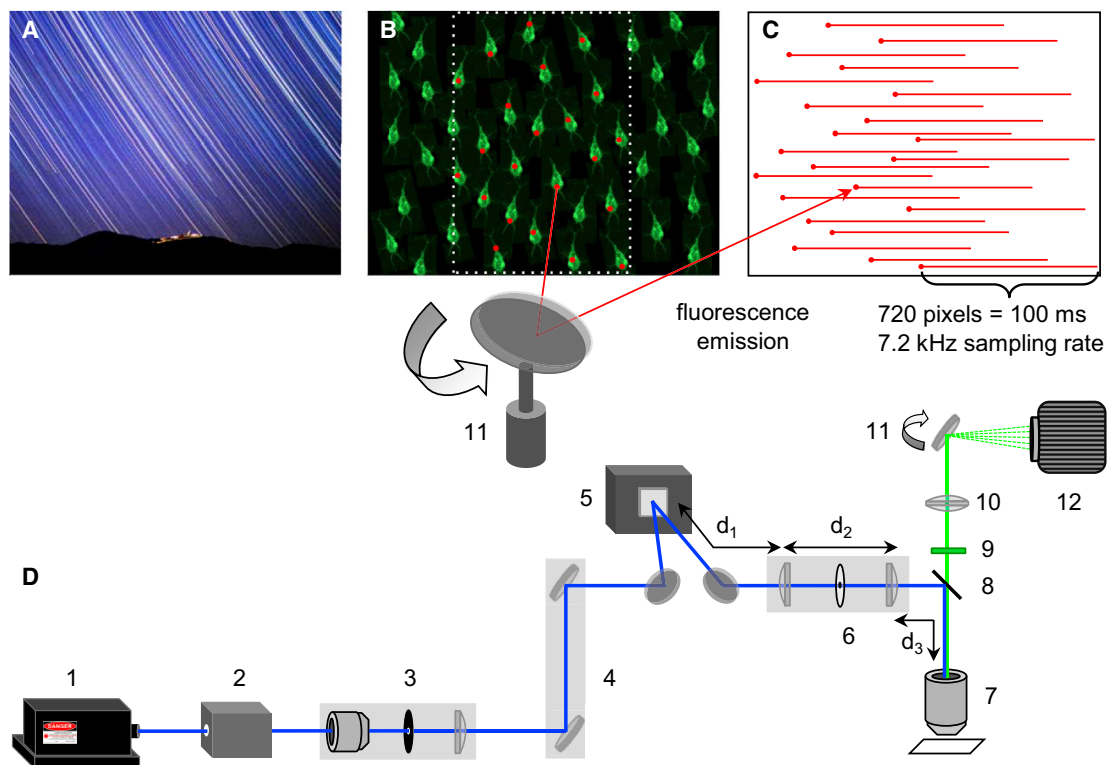

FIGURE 1 Achieving subframe rate temporal resolution through streaking. (*A*) The earth's rotation produces star trails in long camera exposures of the night sky (courtesy of Capella Observatory (36)) (*B*) The schematic depicts a custom pattern of excitation spots (*red dots*) created using an SLM, targeting neurons labeled with a fluorescence dye (*green*) in the middle half of the field of view. (*C*) The fluorescence from each target is streaked across half of the CMOS sensor by scanning the mirror to create fluorescent trails, which for a 100 ms exposure achieves a sampling rate of ~7.2 KHz. A schematic of the FTM optical path is shown in (*D*). The intensity of 488 nm diode laser (1) beam is modulated by an AOTF (2) and then collimated and expanded by a spatial filter (3) before ascending up a periscope (4). The laser is reflected off an SLM (5), whose image is projected by a pair of planoconvex lenses (*with beam block*) (6) onto the back focal plane of the objective (7) by properly setting the distances d$_1$, d$_2$, and d$_3$ (see Materials and Methods). The microscope's dichroic mirror (8) and emission filter (9) allow fluorescent light to pass into the custom housing, where an achromatic doublet (10) and galvanometer-driven mirror (11) focuses and streaks the light respectively, onto the camera sensor (12). To see this figure in color, go online.

isoflurane and decapitated, and coronal brain slices (300 μm) were cut in an ice cold (4°C), low-sodium cutting solution using a vibratome (Leica VT-1000, Leica Microsystems, Buffalo Grove, IL). Slices were incubated for ~30 min at 35°C and allowed to acclimate to room temperature before electrophysiological and optical recordings were made. Cutting and recording media were bubbled with 95% O_2 and 5% CO_2. The low-sodium cutting solution consisted of (in mM): 82.7 NaCl, 2.4 KCl, 1.4 NaH2PO4, 0.5 CaCl2, 6.8 MgCl2, 23.8 NaHCO3, 65 sucrose, and 23.7 glucose.

Organotypic slices were prepared using the interface method (20) using a similar protocol for cutting slices as described previously, with the exception of using 400 μm thick slices from 7-day-old Sprague-Dawley rats. Each slice was placed on a cell culture insert with two attached electrodes and positioned so that the electrodes were under the slice with the tips separated by 2 mm and located 400–800 m from the cortical surface (21). Culture medium was changed 1 and 24 h after cutting and every 2–3 days thereafter. Cutting medium consisted of Eagle's minimum essential medium (EMEM; catalog no. 15-010, MediaTech, Herndon, VA) plus (final concentration in mM) 3 $MgCl_2$, 10 glucose, 25 HEPES, and 10 Tris base. Culture medium consisted of EMEM plus (final concentration in mM) 1 glutamine, 2.6 $CaCl_2$, 2.6 $MgSO_4$, 30 glucose, 30 HEPES, 0.5 ascorbic acid, 20% horse serum, 10 units/l penicillin, and 10 g/l streptomycin. Slices were incubated in 5% CO_2 at 35°C for 14–22 days before experimentation.

Electrophysiology

Whole cell recordings were made from cortical pyramidal neurons visualized using an upright microscope (Olympus BX-41, Olympus America, Center Valley, PA) with a 20× water immersion objective (Olympus XLUMPLFL20XW, N.A. 0.95) using oblique illumination delivered slightly off axis via the condenser. Experiments were carried out at room temperature and 30°C for acute and organotypic brain slice experiments, respectively. Artificial cerebrospinal fluid (ACSF) consisting of (in mM, for acute): 119 NaCl, 2.5 KCl, 1.25 NaH_2PO_4, 2 $CaCl_2$, 1 $MgCl_2$, 26 $NaHCO_3$, and 25 glucose, or (in mM, for organotypic): 125 NaCl, 5.1 KCl, 1 NaH_2PO_4, 2.6 $CaCl_2$, 2.6 $MgSO_4$, 26.1 $NaHCO_3$, and 25 glucose was perfused at a rate of 3 ml/min. The internal solution for whole cell recordings contained (in mM): 126 $KMSO_3$, 10 KCl, 4 NaCl, 10 HEPES, 0.5 EGTA, 14 Tris-phosphocreatine, 2 MgATP, 0.4 NaGTP, or (in mM, for organotypic): 100 K-gluconate, 20 KCl, 10 HEPES, 10 Disodium-phosphocreatine, 4 ATP-Mg, 0.3 GTPNa, and was adjusted to pH 7.3 and 290–300 mOsm. An Axopatch 200A was used to record electrophysiological signals filtered at 2 to 5 kHz, which were digitized (20 kHz) by analog to digital converter (USB 6259, National Instruments, Austin, TX). In voltage clamp, the pipette and cellular capacitance were compensated for using onboard circuitry. Data for intracellular recordings was acquired using electrophysiology software (WinWCP, University of Strathclyde, Glasgow, Scotland) for intracellular recordings. Experiments were analyzed using custom routines written in MATLAB (The MathWorks, Natick, MA) and electrical recordings were filtered in software at 2 kHz.

Fluorescent probe labeling

Individual cells in acute brain slices were labeled with DiO-C18 or DiO-C16 (Biotium, Hayward, CA) via patch pipette as previously described (3,18). Briefly, stock solutions of DiO were prepared at 1.5 mM in dimethyl sulfoxide (DMSO). Internal solution with a final concentration of 1.5 μM DiO was prepared from the stock at least daily, maintained on ice to minimize hydrolysis of ATP, and sonicated and vortexed just before backfilling each patch pipette. As noted previously (3,18) having visible accumulation of dye crystal at the tip of the pipette maximizes the success of labeling. All cells were labeled with DiO and recorded in whole cell configuration with the same intracellular electrode (3–7 MΩ). DPA (City Chemical, West Haven, CT) was bath-applied at 2 to 3 μM in ACSF for >30 min before

the start of experiments, and freshly diluted each day from a 20 mM stock in DMSO (Sigma-Aldrich, St. Louis, MO).

Cells in organotypic slices were bulk labeled with OGB-AM1 via glass electrode as described previously (22). Briefly, a 2 mM stock solution of OGB-AM1 in 10% Pluronic F-127/DMSO was diluted in ACSF to a final concentration of 200 μM and loaded into a patch pipette. Under visualization, the pipette was lowered into the perfused slice and positive pressure was applied (~0.5 psi) while the pipette was parked in the extracellular space for ~2 min. The pipette was withdrawn and fluorescence was monitored for adequate labeling (15–30 min) while continuing to perfuse the slice with ACSF. Although for some experiments individual cells bulk labeled with OGB-AM1 were patched and recorded intracellularly, internal solution dilutes the OGB-AM1 yielding smaller amplitude Ca^{2+} fluorescence signals (see Fig. 3). For single cell Ca^{2+} experiments measurements, the cell impermeable formulation OGB-1 was used. Here, a 10 mM stock of OGB-1 in water was diluted in internal recording solution to a final concentration of 100 μM. These cells were filled with dye via the patch pipette and recorded in the whole cell configuration.

For control experiments using fluorescent beads, fluorescent polystyrene microspheres (200 nm, green, Molecular Probes – Life Technologies, Eugene, OR) were diluted into water (~1000-fold) and sparsely evaporated onto 18 mm coverslips. Fluorescence slides were custom made by laser cutting 18 mm circles from fluorescent acrylic sheets (green, 85635K411, McMaster-Carr, Santa Fe Springs, CA) and imaged 3 to 4 μm below the surface.

Optical measurements

A schematic of the optical path is shown in Fig. 1. The beam from a 488 nm diode laser (PhoxX 488-60, Omicron Laserage Laserprodukte, Rodgau-Dudenhofen Germany), whose intensity (~15 to 30 μW per excitation spot) is modulated with an acoustic optical tunable filter (AOTF, TF525-250-6-3-GH18A, Gooch & Housego, Moorpark, CA) is collimated and expanded with a spatial filter (Zeiss A-plan 10× objective 0.25 NA, 5 μM pinhole P5S Thorlabs, planovonvex lens fl = 75mm, LA1608-A, Thorlabs, Newton, NJ) to fill the LCOS-SLM (X10468-01, Hamamatsu Photonics K.K., Bridgewater, NJ). A periscope raises the height of the beam to match the height of the epifluorescent path of the microscope. A pair of plano-convex lenses (fl = 200 mm, LA1708-A, Thorlabs) form a telescope, projecting the image of the SLM onto the back focal plane of the objective (Olympus XLMUMP 20X, N.A. 0.95) while maintaining beam collimation and filling the back aperture (see Fig. 1, d1 = 264 mm, d2 = 400 mm, d3 = 136 mm). A beam block consisting of a 500 μm diameter metallic chrome spot with 4+ optical density deposited onto a BK-7 circular glass slide (3I, Inc. Denver, CO) sits at the intermediate focus of the telescope and blocks undiffracted light from reaching the sample. The diameter of the objective's back aperture and the width of the SLM are comparable. Thus, in this configuration beam expansion by the telescope is not required. Lens free access to the dichroic filter (z488rdc-xr, Chroma Technology, Bellows Falls, VT) is achieved by removing the microscope's fluorescence illuminator attachment, leaving the filter cube turret in place. Standard wide-field images are captured by whole field laser illumination via the SLM. Commercially available software (Slidebook, 3I, Inc.) is used for image acquisition, calculating the phase map for the desired pattern of excitation spots as previously described (16), and communicating to the SLM via a digital video interface. Fluorescence light is long pass filtered (HQ500LP emission filter, Chroma Technology) before reaching the tube lens (achromatic doublet fl = 200 mm, Thorlabs); emitted light is then reflected by a galvanometer-driven elliptical mirror (scanner: 6240HM40B, mirror: short axis diameter = 30 mm, 6M2430X40S100V1, Cambridge Technology, Bedford, MA). The tube lens and mirror are contained within a custom housing attached to the emission port of fluorescence turret. The fluorescence is imaged onto a CMOS camera (ORCA-Flash 2.8 C11440-10C, Hamamatsu Photonics K.K.) mounted to the distal end of the housing. The galvanometer

driven mirror and servo driver card (67124H30-1, Cambridge Technology) are controlled by a custom circuit containing a microcontroller (Atmel 8515, San Jose, CA) and a digital to analog convertor (Texas Instruments, DAC712, Dallas, TX) and custom software. Electrophysiology software (WinWCP) coordinates the timing of the electrophysiology data acquisition (digital to analog timing 100 kHz), and triggers the AOTF, camera, and microcontroller-controlled mirror. For experiments requiring more precise timing (see Fig. 2 E), the electrophysiology software triggered a signal generator (ORTEC, Oak Ridge, TN) to deliver pulses delayed by 100 μs increments. Although continuous image acquisition and scanning of the mirror is straightforward for frame transfer cameras, the CMOS camera uses a rolling shutter allowing for streaking of fluorescence in one direction only. Thus, fluorescent streaks were acquired in single frames (gain 1×)

lasting between 100 and 600 ms depending on the experiment, with 1 to 3 s between frames assuring that fluorescence changes return to resting value before the subsequent frames.

Data analysis

All imaging data were analyzed offline using custom routines written in MATLAB. An image frame containing a pair of laser pluses (0.1 to 0.5 ms in duration) were used to mark the location (timing) of the streak onset and termination. This timing, as well as the duration of the laser exposure during all subsequent frames was recorded concurrently by the electrophysiology software. Baseline streaks lacking electrophysiological
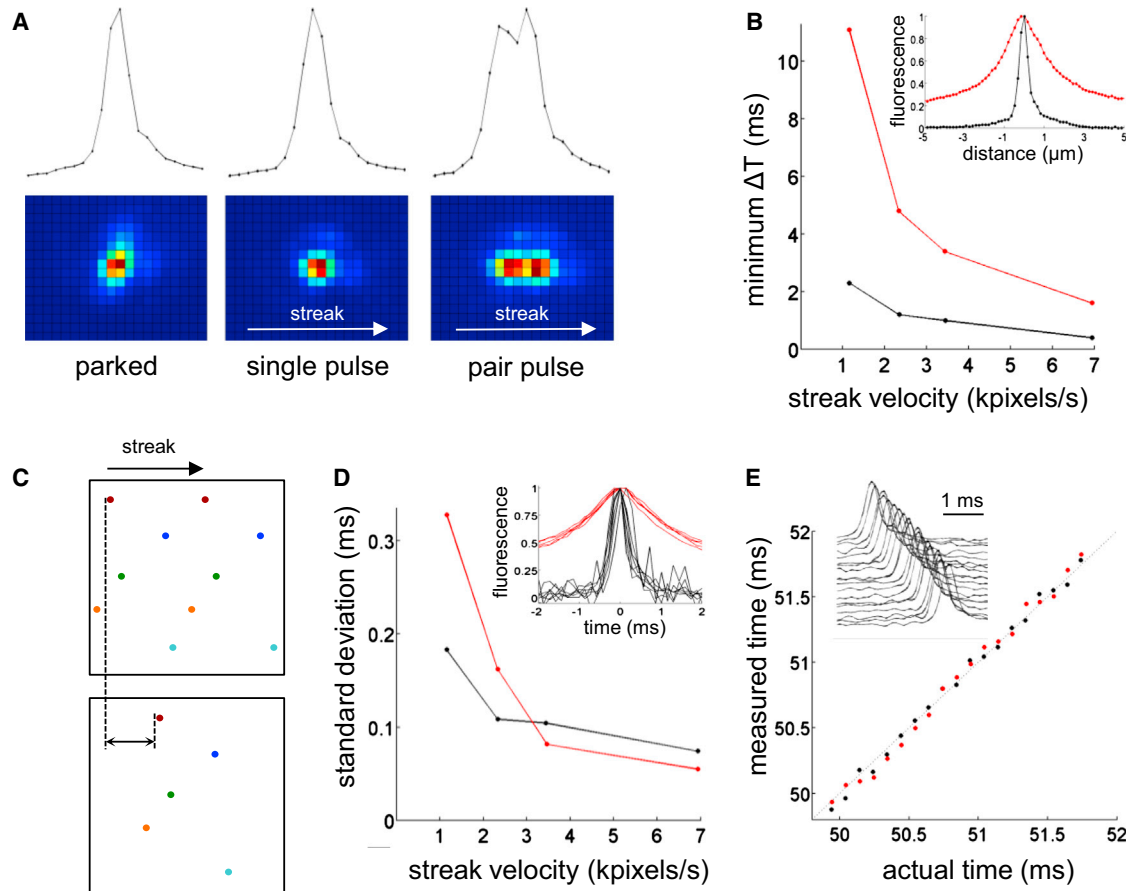

FIGURE 2 Characterization of the time resolution of the FTM. (*A*) Left panel shows an image of a 200 nm fluorescent bead illuminated with a near diffraction-limit laser spot, with the mirror parked. Middle and right panels show images of the same bead being streaked at ~7000 pixels/s illuminated with a single and pair (400 μs apart) of 50 μs laser pulses, respectively. Above each image is the fluorescence intensity plotted along the direction of the streak. (*B*) Plot of the minimum time required to resolve a pair of laser pulses illuminating fluorescent beads (*black*) and fluorescent acrylic slide (*red*) for varying mirror velocities (error bars lie within the points, see Materials and Methods). The minimum ΔT is defined arbitrarily as the minimum separation that yields a local minimum in the fluorescence intensity profile along the streak with a peak to trough height >10σ, where σ is the standard deviation of the fluorescence noise. Inset shows the size of the laser spot illuminating a bead (*black*) and a fluorescent acrylic slide ~3 μm below the surface (*red*). (*C*) Schematic of experimental procedure for measuring the precision with which the FTM can determine the timing of events. Laser spots illuminate a collection of beads (*each depicted with a different color*) within the field view while the image is streaked with laser pulses marking the start and end of the streak (*depicted with a pair of spots of the same color*). In the subsequent frame, the image is streaked again with a single laser pulse delivered at approximately the middle of the streak. The timing of each spot from the start of the streak is measured for each bead. (*D*) The standard deviation of these times is plotted as a function of mirror velocity, for laser spot illuminated beads (*black*) and a fluorescent acrylic slide (*red*). Inset plots the normalized fluorescence intensities along each streak for a collection of spots targeted onto beads (*black*) and a fluorescent slide (*red*). (*E*) Plot of the position of a single spot illuminated bead (*black*) and fluorescent slide (*red*) streaked at ~7000 pixels/s and excited with a single laser pulse that is delayed by 100 μs increments in consecutive frames. The dashed line $y = x$, represents perfect agreement. Inset shows streak profiles (*gray*) for the bead along with the smoothed fits (*black*) in consecutive frames. To see this figure in color, go online.

stimuli were used to characterize the streak shape and subtract any static intensity variation along the streak. In some experiments the baseline was calculated by fitting the portions of the streak that were free of electrophysiological stimuli to a fourth or fifth degree polynomial. Both methods resulted in profiles that were consistent between frames and were used primarily to remove the rising and falling edges of the streak profile. In a minority of experiments, minimal fluorescence scattering from the rising or falling edge of neighboring streaks located in close proximity could be observed in the baseline streaks, and subtraction of baseline streaks was effective in removing this effect, which was entirely consistent between frames.

Fluorescence traces from electrophysiology experiments were low pass filtered at 1 kHz. $\Delta F/F$ was calculated by subtracting the mean fluorescence value F, which was calculated over portions of the streak lacking electrical stimuli, and then dividing by F. Depolarization of the cell results in a decrease in fluorescence of DiO-DPA (3,18), and fluorescence traces were inverted to match electrophysiological convention. The SNR was calculated by dividing the peak stimulus evoked fluorescence change by the standard deviation (σ) of the fluorescence signal over a 20 ms window. For timing measurements, fluorescent traces were smoothed using a spline smoothing routine in MATLAB. For experiments using OGB-1, single action potentials result in a fluorescence increase with a sigmoid-like function, and the timing of APs was defined as the time at which the fluorescence signal crosses 50% of the maximum stimulus-induced fluorescence. For control experiments measuring the timing of delta function responses and DiO-DPA experiments reporting neuronal action potentials, the timing of individual events was marked by the peak in the smoothed fluorescence fluctuation. For the control experiments (see Fig. 2 B) the minimum separation time (ΔT) is quite reproducible, with the fluctuations between trials smaller than the 100 μs increments used to find the minimum ΔT. Thus, the error bars for Fig. 2 B were conservatively set to 100 μs. For comparison of action potential arrival times (Fig. 4 E), a paired t-test was used to determine the significance of the difference.

RESULTS

Current scientific cameras sensitive enough for fluorescence microscopy can capture and process light intensity information from ~10^7 to 10^8 pixels/s (~1 megapixel sensor at 10-100Hz frame rate). However, due to the modestly sparse and irregular distribution of fluorescent targets in a typical biological experiment, the vast majority of these pixels carry no biologically relevant information. We designed the FTM to make efficient use of this bandwidth by using a portion of these unused pixels to capture time varying fluorescence from targets of interest. A schematic of the FTM is depicted in Fig. 1. First, a wide-field epifluorescence image is taken of the specimen, such as a neuronal network labeled with fluorescent probes. Fluorescently labeled targets of interest are identified, and using commercially available software (Slidebook, 3I Inc.) implementing previously described algorithms (16) a custom pattern of nearly diffraction-limited excitation points is created using the SLM. The resulting fluorescence image is projected onto approximately half of the camera sensor, typically with megapixel or greater resolution. Finally, a linear galvanometer in the emission path creates fluorescent trails by streaking the fluorescence signal emanating from each point into a line across the camera sensor. The mirror movement is synchronized to the camera acquisition, and the resulting movie of fluores-

cent trails can capture temporal information with sub-millisecond resolution in micron sized cellular compartments. For example, using our scientific CMOS camera (ORCA Flash 2.8, Hamamatsu), scanning across half of the 1440 vertical pixels in 100 ms yields a sampling rate of ~7 kHz, which is sufficient to capture the fastest neuronal signals. However, as we discuss below streaking a finite-sized spot across the sensor convolves or smooths out the fluorescence dynamics, and places limitations on the temporal resolution of the technique.

To characterize the capabilities and limitations of the FTM, we illuminated fluorescent beads with an excitation spot generated by the SLM and pulsed the laser for a known duration while streaking the resulting fluorescence across the camera sensor. Fig. 2 A shows the fluorescence streak resulting from a subdiffraction limit sized (200 nm) bead excited with a 50 μs duration laser pulse used to approximate a delta function. Due to diffraction, the streak resulting from the fluorescence impulse is not sized infinitesimally thin, but rather has a profile equivalent to the image of a subdiffraction limit sized bead, which approximates the point spread function (PSF) that defines the spatial resolution of the microscope (inset Fig. 2 B). The Raleigh criteria states that the width of the PSF places a lower limit on how close two diffraction limited objects can be located in space and be distinguished as separate objects. Likewise, for the FTM, the PSF places a lower limit describing how closely two infinitesimally short pulses illuminating a subdiffraction limit sized object can occur consecutively in time and be resolved as separate events. In practice, most objects illuminated with the same excitation spot will produce a larger image than that of the subdiffraction bead, and generate streaks with slower time resolution. The resulting time varying fluorescence fluctuation as measured by the streak technique is a convolution of the actual fluorescence dynamics with shape of the object. Thus, the separation time necessary to resolve a pair of consecutive fluorescence events increases with the increasing size of the object (Fig. 2 B). In principle one can attempt to deconvolve the streak with the object shape, but in practice this results in only a modest change in the fluorescence profile and comes at the cost of SNR, which is the primary consideration in the detection of APs. Finally, increasing the speed of the galvanometer and the resulting streak, improves the ability to resolve closely separated fluorescence fluctuations in time regardless of the size of the object (Fig. 2 B).

In contrast, the Raleigh criteria places no limits on the precision with which one can measure the position of objects. For example, studies using fluorescence microscopy to track the location of single molecules can localize an object's location or center of mass with subpixel and often nanometer resolution, well below the diffraction limit (23). Analogously in FTM, neither the convolution induced by streaking nor the PSF limit the resolution with which one can assign the timing of fluorescent events within the field

of view. This is limited primarily by SNR. To explore this precision, we used the FTM to illuminate a group of fluorescent beads, each illuminated with an individual excitation spot, and then measured the distribution of arrival times of a delta function laser pulse that illuminates all the beads simultaneously (Fig. 2, *C* and *D*). Again, the resulting fluorescence change is equivalent to the PSF, whose peak can be localized with subpixel resolution ($\sigma = < 100$ μs, for streak with velocity of ~7000 pixels/s). We also delayed the arrival of the laser pulse in subsequent frames by a fixed incremental amount, demonstrating that the relative timing of events can be reliably measured within ~50 μs (Fig. 2 *E*, root mean-square about the line $y = x$, representing perfect agreement is 46 μs and 60 μs for the fluorescent beads and slide, respectively). Thus, unlike the time resolution needed to resolve consecutive fluorescence fluctuations, the ability to measure the timing of an event is more precise and relatively insensitive to the size of the object being illuminated.

We next set out to determine the capability of the FTM to resolve single APs in a collection of individual neurons in a cortical slice culture preparation labeled with the fluorescent Ca^{2+} reporter OGB1-AM. Here, excitation spots were targeted to selected neurons bulk loaded with OGB1-AM, while intracellular electrical signals were recorded simultaneously from one of the targeted cells (Fig. 3). To excite sufficient population activity in the preparation, individual 200 μs electrical pulses were delivered through stimulation electrodes embedded under the slice and whose amplitude was titrated until single APs were reliably elicited in the electrically recorded cell. The fluorescent changes of OGB1-AM and the underlying Ca^{2+} dynamics, which are a surrogate for neuronal activity are an order of magnitude or more slower that the AP itself (exponential rise time: ~8 ms, exponential decay constants: fast 56 $\pm$ 3 ms and slow 777 $\pm$ 80 ms (12)). The FTM can clearly resolve the change in fluorescence associated with individual APs in the electrically recorded cell as well as putative single APs in the remaining cells with a SNR of ~100 (Fig. 3 *C*). Notice that the fluorescence appears to rise ~30 ms before the onset of the first action potential. This is another consequence of the convolution of the time-dependent fluorescence signal with the spatial profile of the fluorescent spot (average decay to 10% of its peak value in 80 pixels = 33.6 ms), which distributes light both forward and backward in time along the streak. However, the convolution does not alter the timing (location) of the fluorescence fluctuation. To assess the ability of the FTM to capture the relative timing of APs, we measured the distribution of arrival times of the AP induced rise in fluorescence in the neurons. Despite the slow dynamics of OGB1-AM, the arrival times of the simultaneously evoked APs agree within $\sigma = 1.2$ ms. This also demonstrates that the optical cross talk between target cells is minimal, as neighboring streaks are offset in location along the sensor axis that represents time, and any cross talk would degrade this precision. To further assess the ability of
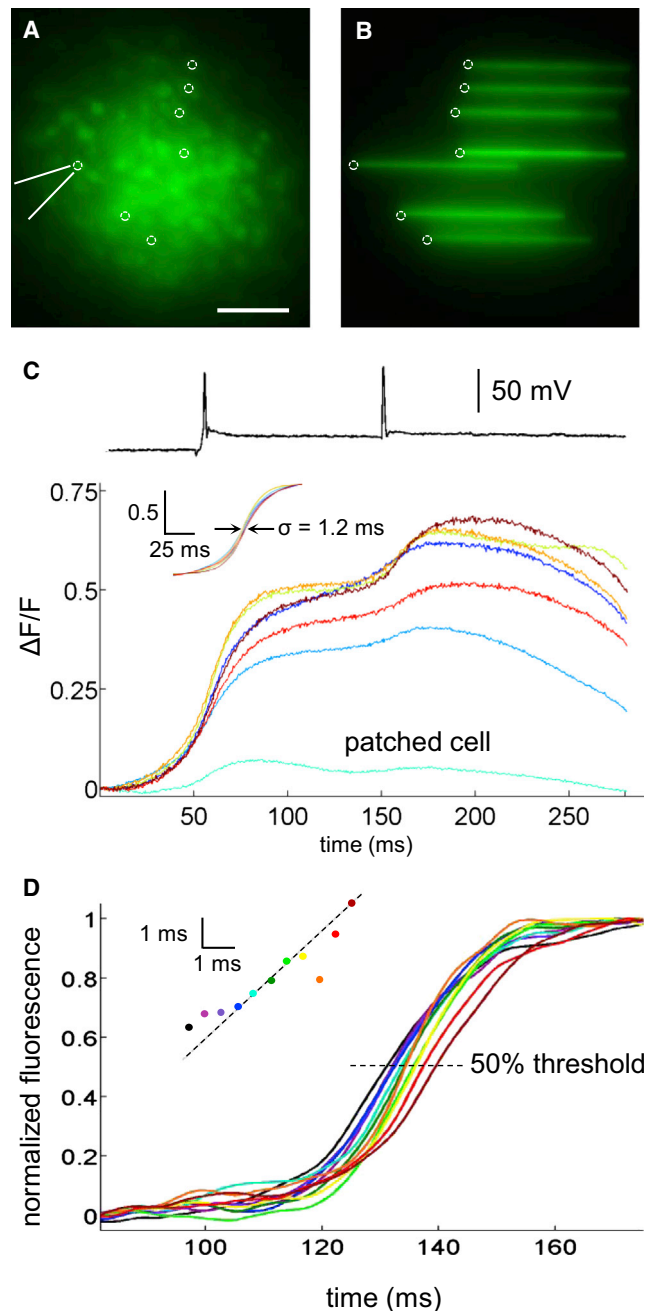

FIGURE 3 FTM can detect Ca^{2+} influx reported via OGB1 from single action potentials with precise timing. (*A*) Wide-field and (*B*) streak fluorescence image of a collection of cells in organotypic slice culture, including a single patched cell on the left, bulk labeled with OGB1-AM. (*C*) Field stimulation with individual 200 μs pulses separated by 100 ms induce single APs that are recorded via the patch pipette (*above*) and streak fluorescence (*below*). Inset: normalized and smoothed fluorescence responses to first AP in nonpatched cells show precise timing with a $\sigma = 1.2$ ms. (*D*) Normalized and smoothed fluorescence responses of a single cell loaded with OGB1 via patch pipette, and stimulated under current clamp to fire single APs that are delayed by 1 ms increments in consecutive frames. The inset plots the time to reach 50% fluorescence versus the time of the AP. The dashed line $y = x$, represents perfect agreement. To see this figure in color, go online.
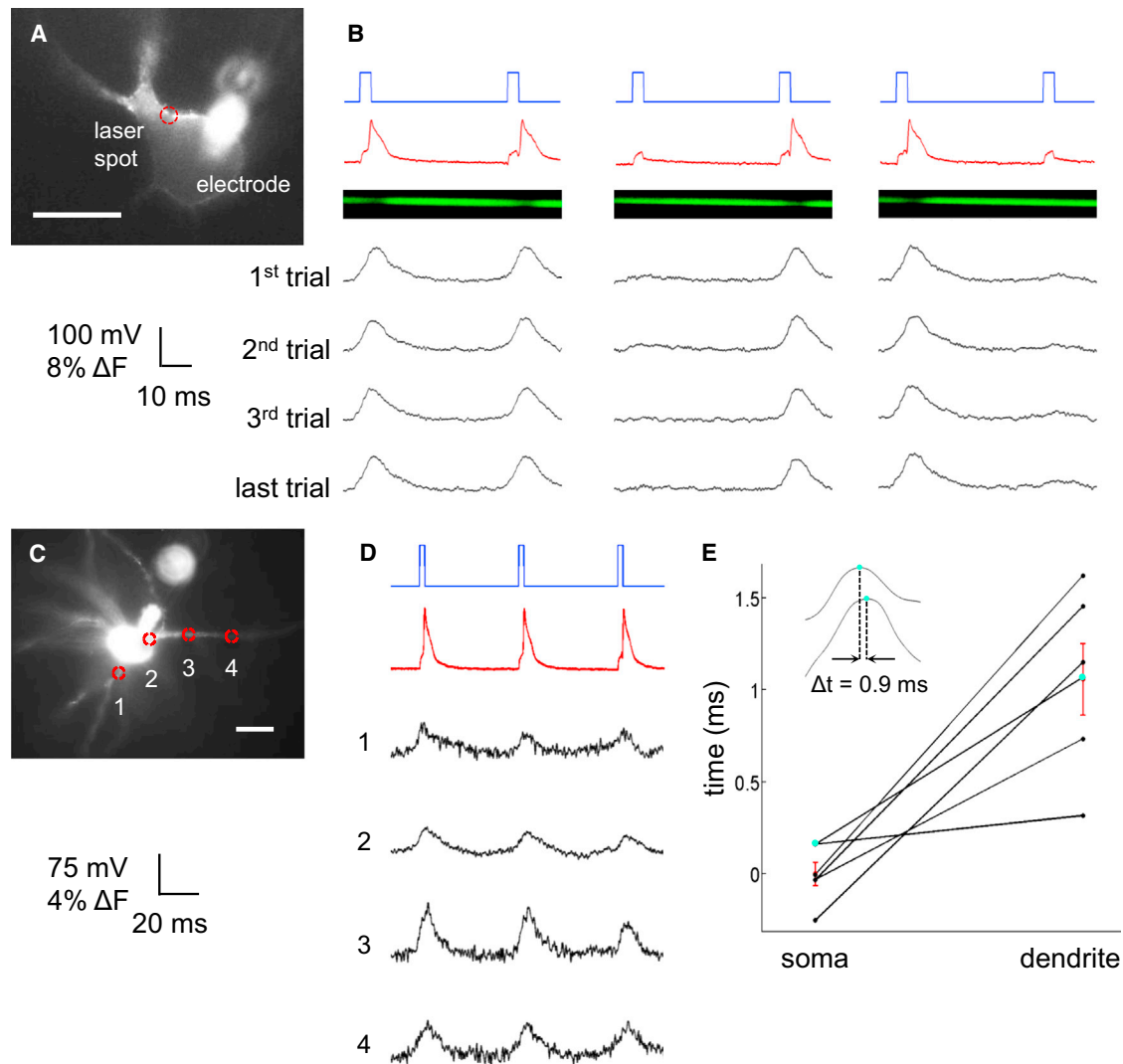
FIGURE 4 FTM exhibits both the time resolution and sensitivity necessary to capture precisely timed optically reported APs at multiple locations. (*A*) Epifluorescence image of a cortical neuron labeled with DiO-DPA via glass electrode. Scale bar 15 μm. (*B*) Pair of 1 nA current pulses delivered 50 ms apart (*blue*) result in a pair of APs and failures as seen in the voltage trace (*red*) as well as the inverted fluorescence traces (*black*, showing the first three and last trials of each type of response) calculated from streaks such as the example streak shown in green. (*C*) The locations of four simultaneous fluorescence measurements in another cell are marked by red circles. Scale bar 30 μm. (*D*) Three 1 nA current pulses delivered 50 ms apart (*blue*) result in action potentials as seen in the voltage trace (*red*) as well as the inverted fluorescence traces (*black*) at the locations marked in (*C*). (*E*) A plot of the relative arrival times (*black*) for the middle action potential show a delay at the distal dendrite ~70 um away. Average delay and error bars (SE) shown in red. *P*-value = 0.006, paired *t*-test. Inset shows an example (*light blue points*) of a smoothed action potential at each location showing a delay in the timing of the peak of 0.9 ms. To see this figure in color, go online.

the FTM to measure the timing of APs reported by Ca^{2+} indicators, we recorded simultaneous electrophysiological and fluorescence signals from a single neuron labeled with OGB-1 while delaying the onset of the induced APs in consecutive trials by 1 ms increments, again demonstrating that the timing of events can be reliably measured within 1.3 ms (Fig. 3 *D*, root mean-square about the line *y = x*).

Although recent advances in voltage-sensitive fluorescent probes such as DiO-DPA allow for reliable detection of individual APs in single neurons (3,18), fluorescence changes in voltage sensors resulting from single APs are typically

too rapid or have inadequate SNR to be detected by multifocal imaging approaches. This is particularly true in highly scattering environments such as brain slices. We tested how well the FTM could reliably resolve single APs reported by the voltage sensor DiO-DPA in acute brain slices. Fig. 4 shows a cortical neuron in an acute brain slice preparation labeled via whole cell pipette via DiO. Fig. 4 *B* shows electrophysiological data from a neuron being stimulated in the presence of 3 μM DPA with pairs of current pulses delivered 50 ms apart along with the simultaneous fluorescence intensity of DiO-DPA captured by the FTM. The intensity of the

TABLE 1 FTM can achieve tens of kHz sampling rates and greater

Camera	Sensor type	Max Q.E.	Read noise (e rms)	Resolution	Full frame rate (Hz)	FTM sampling rate (kHz)
ORCA Flash 2.8	CMOS	>0.65	3[a]	1920 × 1440	45	32.4[b]
ORCA Flash 4.0	CMOS	>0.7	1.9	2048 × 2048	100	102.4[b]
Zyla 5.5	CMOS	0.6	2.6	2560 × 2160	40	43.2[c]
Evolve 512 Delta	EMCCD	>0.9	<1[d]	512 × 512	62.5	16

A wide selection of commercially available cameras can be adapted for FTM to achieve optimal performance. FTM sampling rate calculated as maximum full frame rate × (number of pixels in 1D)/2. Faster rates can be achieved by lengthening streaks or using less than the full exposure time. EMCCD, electron multiplying charge-coupled device.

[a]With gain 8×.
[b]Rolling shutter allowing only discontinuous scanning.
[c]Values for global shutter mode allowing continuous scanning.
[d]With EM gain.

current injections was chosen to be near threshold to achieve roughly equal probability of spike failures and successes. Under these circumstances the FTM reliably captures every spike and failure during all 37 trials. The maximum SNR of 43 achieved in these traces (Fig. 4 B, average SNR = 32.9 ± 1.4 SE) is significantly better than previous single point measurements of APs with this probe (3,18). Next, we tested whether the FTM could resolve single APs at multiple locations within a neuron by recording back propagated APs in dendrites. Fig. 4 D shows that single APs can be resolved in processes ~70 μm away from the cell body without averaging (2 μM DPA). Delays in the arrival time of the AP at the distal dendrite could be resolved and allow us to estimate a propagation velocity of ~0.1 m/s at room temperature, consistent with previous studies (24). Thus, the FTM exhibits both the time resolution and sensitivity necessary to capture precisely timed neuronal APs at multiple locations without the need for averaging.

DISCUSSION

The FTM makes efficient use of the camera's bandwidth and excess spatial resolution to sample temporal dynamics at rates that are orders of magnitude faster than the camera's native frame rate. In contrast to scanning laser techniques, FTM's excitation light is scanless and measures photon flux continuously and in parallel from all targets. This minimizes photon shot noise by maximizing the number of photons collected for a given sampling rate, while avoiding areas of nonspecific fluorescent labeling. Thus, for photon-limited experiments, as the number of fluorescent targets N increases, the FTM has a greater than $\sqrt{N}$ improvement in SNR over rapid scanning techniques that measure fluorescence from targets in series (12).

The STM also allows one to optimize the size of the excitation spot to suit different experiments. Exciting near diffraction-limited regions of interest (16) provides optimal two-point temporal discrimination (Fig. 2 B) and allows for measurements in subcellular structures such as neuronal processes and small volumes necessary for single-molecule experiments. In contrast, using larger regions of interest maximizes photon collection and SNR, with minimal degra-

dation of absolute timing measurements (Fig. 2 D). Larger excitation spots, however, limit two-point temporal discrimination as well as the number of targets that can be imaged without cross talk due to scattering. The largest contaminant from neighboring streaks is fluctuations arising from action potential induced changes in fluorescence, quantified as ΔF/F. Any fluorescence contributions that are not dependent on time are subtracted out, and contributions due to noise are small when working with SNRs sufficiently >1. One can set an arbitrary, yet reasonable threshold allowing 10% contamination of a given streak's signal from a neighboring streak. Assuming that the mean fluorescence F and the action potential induced changes in fluorescence ΔF of all the spots are similar, then one only need consider the separation distance at which a steak's fluorescence intensity decays to 10% of its peak value. For the experiments using DiO-DPA in Fig. 4 C the average spot decays to 10% in 36 pixels (halfwidth), yielding ~27 spots per full field of view. Experiments using OGB1-AM such as those in Fig. 3 C have more diffuse labeling and spots decay to 10% at a mean distance of 80 pixels, yielding ~12 spots per full field of view. For experiments in low scattering environments such as cell culture the number of achievable targets is on the order 10^2. There are several modifications to the microscope including a rotating housing containing the emission optics that could be implemented to optimize the streak direction and the maximum number of targets. However, in practice the number of labeled targets within the field of view in the same focal plane is often less than the maximum number estimated previously.

We demonstrate the use of the FTM by measuring multifocal optically reported neuronal signals including individual action potentials. The favorable attributes of the FTM described previously make it suitable for a diverse range of applications requiring multifocal photometry. In addition, the FTM is camera independent and can exploit the improving and growing number of available sensor technologies, yielding sampling rates up to ~100 kHz with full-frame illumination (Table 1). For experiments where continuous illumination for extended periods of time is not needed, one can streak the fluorescence during a fraction of the camera's full exposure time. Here, the speed and

sampling rate is only limited by the mechanical properties of the mirror and the system used to drive it. Depending on the size of the mirror, scanning times of 100 μs and sampling rates of 10 MHz could be achievable. For the current study, we used a scientific CMOS camera that has a favorable balance of pixel count, frame rate, and readout noise. Alternatively, one could use the FTM to perform high-throughput single molecule experiments, taking advantage of the low noise properties of current electron multiplying charge-coupled device technology while maintaining the fast sampling rates necessary to capture molecular movement or state changes. Possibilities for adapting FTM beyond the experiments described here include multifocal adaptations of spectral imaging (25), fluorescent correlation spectroscopy (26), and single molecule and cell-based Förster resonance energy transfer (FRET) (27,28).

The FTM will likely benefit from the rapid development of genetically targeted voltage sensors, and is well suited to record multicellular network activity in genetically defined neuronal populations. In addition, FTM can be adapted to perform multifocal multiphoton microscopy (MMM). Previous studies have shown that multiphoton microscopy signals can be resolved reliably in highly scattering tissue such as brain slice at depths of 200 μm or more (13). Furthermore, FTM at greater depths may benefit from image processing techniques that assign photons to targets in noisy environments (29–31). Finally, there has been significant effort to develop both red-shifted genetically encoded indicators (7,32) as well as opsins (33,34) that will eventually allow for simultaneous and nonoverlapping activation and detection of neural activity, an endeavor for which the FTM would also provide advantages. In particular, the ability of SLMs to produce activation patterns within a three-dimensional volume (35), suggests that one could use two-photon SLM to stimulate and record activity concurrently from a collection of neuronal targets.

REFERENCES

1. Chen, T.-W., T. J. Wardill, …, D. S. Kim. 2013. Ultrasensitive fluorescent proteins for imaging neuronal activity. *Nature.* 499:295–300.

2. Paredes, R. M., J. C. Etzler, …, J. D. Lechleiter. 2008. Chemical calcium indicators. *Methods.* 46:143–151.

3. Bradley, J., R. Luo, …, D. A. DiGregorio. 2009. Submillisecond optical reporting of membrane potential in situ using a neuronal tracer dye. *J. Neurosci.* 29:9197–9209.

4. Yan, P., C. D. Acker, …, L. M. Loew. 2012. Palette of fluorinated voltage-sensitive hemicyanine dyes. *Proc. Natl. Acad. Sci. USA.* 109:20443–20448.

5. St-Pierre, F., J. D. Marshall, …, M. Z. Lin. 2014. High-fidelity optical reporting of neuronal electrical activity with an ultrafast fluorescent voltage sensor. *Nat. Neurosci.* 17:884–889.

6. Han, Z., L. Jin, …, V. A. Pieribone. 2013. Fluorescent protein voltage probes derived from ArcLight that respond to membrane voltage changes with fast kinetics. *PLoS ONE.* 8:e81295.

7. Hochbaum, D. R., Y. Zhao, …, A. E. Cohen. 2014. All-optical electrophysiology in mammalian neurons using engineered microbial rhodopsins. *Nat. Methods.* 11:825–833.

8. Ducros, M., Y. Goulam Houssen, …, S. Charpak. 2013. Encoded multi-site two-photon microscopy. *Proc. Natl. Acad. Sci. USA.* 110:13138–13143.

9. Sjulson, L., and G. Miesenböck. 2007. Optical recording of action potentials and other discrete physiological events: a perspective from signal detection theory. *Physiology (Bethesda).* 22:47–55.

10. Peterka, D. S., H. Takahashi, and R. Yuste. 2011. Imaging voltage in neurons. *Neuron.* 69:9–21.

11. Cheng, A., J. T. Gonçalves, …, C. Portera-Cailliau. 2011. Simultaneous two-photon calcium imaging at different depths with spatiotemporal multiplexing. *Nat. Methods.* 8:139–142.

12. Grewe, B. F., D. Langer, …, F. Helmchen. 2010. High-speed in vivo calcium imaging reveals neuronal network activity with near-millisecond precision. *Nat. Methods.* 7:399–405.

13. Niesner, R., V. Andresen, …, M. Gunzer. 2007. The power of single and multibeam two-photon microscopy for high-resolution and high-speed deep tissue and intravital imaging. *Biophys. J.* 93:2519–2529.

14. Koester, H. J., D. Baur, …, S. W. Hell. 1999. Ca2+ fluorescence imaging with pico- and femtosecond two-photon excitation: signal and photodamage. *Biophys. J.* 77:2226–2236.

15. König, K. 2000. Multiphoton microscopy in life sciences. *J. Microsc.* 200:83–104.

16. Lutz, C., T. S. Otis, …, V. Emiliani. 2008. Holographic photolysis of caged neurotransmitters. *Nat. Methods.* 5:821–827.

17. Nikolenko, V., B. O. Watson, …, R. Yuste. 2008. SLM microscopy: scanless two-photon imaging and photostimulation with spatial sight modulators. *Front Neural Circuits.* 2:5.

18. Fink, A. E., K. J. Bender, …, D. A. DiGregorio. 2012. Two-photon compatibility and single-voxel, single-trial detection of subthreshold neuronal activity by a two-component optical voltage sensor. *PLoS ONE.* 7:e41434.

19. Smith, S. L., and T. S. Otis. 2005. Pattern-dependent, simultaneous plasticity differentially transforms the input-output relationship of a feedforward circuit. *Proc. Natl. Acad. Sci. USA.* 102:14901–14906.

20. Johnson, H. A., and D. V. Buonomano. 2007. Development and plasticity of spontaneous activity and Up states in cortical organotypic slices. *J. Neurosci.* 27:5915–5925.

21. Johnson, H. A., and D. V. Buonomano. 2009. A method for chronic stimulation of cortical organotypic cultures using implanted electrodes. *J. Neurosci. Methods.* 176:136–143.

22. Takahashi, N., N. Oba, …, Y. Ikegaya. 2011. High-speed multineuron calcium imaging using Nipkow-type confocal microscopy. *Curr. Protoc. Neurosci.*

23. Triller, A., and D. Choquet. 2008. New concepts in synaptic biology derived from single-molecule imaging. *Neuron.* 59:359–374.

24. Stuart, G. J., and B. Sakmann. 1994. Active propagation of somatic action potentials into neocortical pyramidal cell dendrites. *Nature.* 367:69–72.

25. Li, Q., X. He, …, F. Guo. 2013. Review of spectral imaging technology in biomedical engineering: achievements and challenges. *J. Biomed. Opt.* 18:100901.

26. Colyer, R. A., G. Scalia, …, X. Michalet. 2010. High-throughput FCS using an LCOS spatial light modulator and an 8 × 1 SPAD array. *Biomed. Opt. Express.* 1:1408–1431.

27. Marine, S., S. T. Zamiara, …, B. Strulovici. 2006. A miniaturized cell-based fluorescence resonance energy transfer assay for insulin-receptor activation. *Anal. Biochem.* 355:267–277.

28. Arai, Y., and T. Nagai. 2013. Extensive use of FRET in biological imaging. *Microscopy (Oxf).* 62:419–428.

29. Hill, E. S., C. Moore-Kochlacs, …, W. N. Frost. 2010. Validation of independent component analysis for rapid spike sorting of optical recording data. *J. Neurophysiol.* 104:3721–3731.

30. Mukamel, E. A., A. Nimmerjahn, and M. J. Schnitzer. 2009. Automated analysis of cellular signals from large-scale calcium imaging data. *Neuron.* 63:747–760.

31. Cha, J. W., V. R. Singh, K. H. Kim, J. Subramanian, Q. Peng, H. Yu, E. Nedivi, and P. T. C. So. 2014. Reassignment of scattered emission photons in multifocal multiphoton microscopy. *Sci. Rep.* 4:153.

32. Akerboom, J., N. Carreras Calderón, …, L. L. Looger. 2013. Genetically encoded calcium indicators for multi-color neural activity imaging and combination with optogenetics. *Front. Mol. Neurosci.* 6:2.

33. Lin, J. Y., P. M. Knutsen, …, R. Y. Tsien. 2013. ReaChR: a red-shifted variant of channelrhodopsin enables deep transcranial optogenetic excitation. *Nat. Neurosci.* 16:1499–1508.

34. Klapoetke, N. C., Y. Murata, …, E. S. Boyden. 2014. Independent optical excitation of distinct neural populations. *Nat. Methods.* 11: 338–346.

35. Packer, A. M., D. S. Peterka, …, R. Yuste. 2012. Two-photon optogenetics of dendritic spines and neural circuits. *Nat. Methods.* 9:1202–1205.

36. Binnewies, S., and J. Pöpsel. 2009. Startrails above La Silla Observatory, Chile. http://www.capella-observatory.com.